

Lick Spectral Indices for Super Metal-rich Stars¹

A. Buzzoni

*Telescopio Nazionale Galileo, A.P. 565, 38700 Santa Cruz de La Palma, Canary Islands, Spain,
and Osservatorio Astronomico di Brera, Milano Italy*

buzzoni@tng.iac.es

M. Chavez

Instituto Nacional de Astrofísica, Óptica y Electrónica, A.P. 51 y 216, 72000 Puebla, Mexico

mchavez@inaoep.mx

M.L. Malagnini

Dipartimento di Astronomia, Università di Trieste, Via G.B. Tiepolo 11, 34131 Trieste, Italy

malagnini@ts.astro.it

C. Morossi

Osservatorio Astronomico di Trieste, Via G.B. Tiepolo 11, 34131 Trieste, Italy

morossi@ts.astro.it

ABSTRACT

We present Lick spectral indices for a complete sample of 139 candidate super metal-rich stars of different luminosity class (MK type from V to I). For 91 of these stars we were able to identify, in an accompanying paper (Malagnini *et al.* 2000), the fundamental atmosphere parameters. This confirms that at least 2/3 of the sample consists of stars with [Fe/H] in excess of +0.1 dex.

Optical indices for both observations and fiducial synthetic spectra have been calibrated to the Lick system according to Worthey *et al.* (1994), and include the Fe I indices of Fe5015, Fe5270, and Fe5335, and the Mg I and MgH indices of Mg₂ and Mgb at 5180 Å.

Internal accuracy of the observations is found to be $\sigma(\text{Fe5015}) = \pm 0.32 \text{ \AA}$, $\sigma(\text{Fe5270}) = \pm 0.19 \text{ \AA}$, $\sigma(\text{Fe5335}) = \pm 0.22 \text{ \AA}$, $\sigma(\text{Mg}_2) = \pm 0.004 \text{ mag}$, and $\sigma(\text{Mgb}) = \pm 0.19 \text{ \AA}$. This is about a factor of two better than the corresponding theoretical indices from the synthetic spectra, the latter as a consequence of the intrinsic limitations in the input physics, as discussed in Chavez *et al.* (1997).

By comparing models and observations, no evidence is found for non-standard Mg vs. Fe relative abundance, so that [Mg/Fe] = 0, on the average, for our sample.

Both the Worthey *et al.* (1994) and Buzzoni *et al.* (1992, 1994) fitting functions are found to suitably match the data, and can therefore confidently be extended for population synthesis application also to super-solar metallicity regimes. A somewhat different behaviour of the two fitting sets appears, however, beyond the temperature constraints of our stellar sample. Its impact on the theoretical output is discussed, as far as the integrated Mg₂ index is derived from synthesis models of stellar aggregates.

A two-index plot, like Mg₂ vs. Fe5270, is found to provide a simple and powerful tool to probe distinctive properties of single stars and stellar aggregates as a whole. The major advantage, over a classical c-m diagram, is to be both reddening free and distance independent.

Subject headings: stars: abundances – stars: atmospheres – stars: fundamental parameters – Galaxy: stellar content

1. Introduction

A fair recognition of super metal-rich (SMR) stars in the solar neighborhood remains a crucial issue to confidently assess the problem of metallicity estimate in the Galaxy bulge and external galaxies, via population synthesis models.

In the classical works on the subject (Spinrad and Taylor 1969), the definition of SMR candidates mostly relied on the relative chemical abundance with respect to the Hyades and set the nominal threshold for SMR stars at $[\text{Fe}/\text{H}] > +0.2$ dex (that is a metal abundance Z in excess of 50% on the solar abundance).

Both the metallicity scale for the bulge stellar population (Frogel 1999) as well as the individual estimates of Z for the most metal-rich template stars in the disk (first of all the classical SMR standard μ Leo, cf. McWilliam 1997; Taylor 1999; Smith and Ruck 2000) have however been the subject of important revisions in the recent literature, although no conclusive argument seems so far to definitely settle the problem.

In this paper, we follow on the spectroscopic study of a sample of SMR candidates undertaken in Malagnini *et al.* (2000, hereafter Paper I) providing a detailed calibration for the main Lick narrow-band indices in the optical wavelength range. These include the two Mg indices (Mg₂ and Mgb) and the three Fe I indices of Fe5015, Fe5270, and Fe5335 (hereafter referred to in their abbreviated form, i.e. Fe50, Fe52 and Fe53, respectively; cf. Sec. 2).

For most of these stars, we identified in Paper I the photospheric *fiducial* parameters (T_{eff} , $\log g$ and $[\text{M}/\text{H}]$) and computed the corresponding synthetic spectra according to the Chavez *et al.* (1997) theoretical database. Theoretical narrow-band indices will be especially dealt with in Sec. 3, where we address the problem of a possible non-solar $[\text{Mg}/\text{Fe}]$ chemical partition of our SMR candidates.

Metallicity estimate in external galaxies should forcedly rely on population synthesis models by matching integrated indices for the whole stellar aggregate. This is usually done by means of the so-called “fitting function” technique (Worthey *et*

al. 1994, hereafter W94; Buzzoni *et al.* 1992, B92, and Buzzoni *et al.* 1994, B94), that is by fitting index behaviour for local stars and implementing this analytical framework in the synthesis code. It is of paramount importance, in this sense, to confidently validate fitting function predictions also to super-solar metallicity regimes. This is done in Sec. 4, where we check our observations against the W94, B92 and B94 fitting sets.

The Mg₂ vs. Fe52 plot could reveal a simple and powerful tool for stellar diagnostics both for individual objects and stellar aggregates. Its major advantage over the classical c-m diagrams is to be both reddening free and distance independent. In Sec. 5 we will discuss in some detail its possible applications by referring to our stellar sample.

2. Observations and system calibration

The original set of observations of this work consists of 139 bright stars ($V < 8$ mag) in the spectral range between F and M and luminosity class between I and V, selected from three main reference sources for metallicity in the literature.

Dwarf stars (class V-IV) mainly come from the general catalog of Cayrel de Strobel *et al.* (1997), while giants (class III to I) are mostly from Taylor (1991). This two data sources have then be completed with the work of W94 in order to include a set of primary calibrators to the Lick system, and provide a more homogeneous distribution among all luminosity classes.

Each of our SMR candidates is quoted to have *at least* one determination of $[\text{Fe}/\text{H}] \geq +0.1$ from high-resolution abundance studies in the literature.

This working sample has been observed during three runs, between December 1995 and August 1996, at the 2.12m f/12 telescope of the INAOE “G. Haro” Observatory in Cananea (Mexico). We collected Böller and Chivens mid-dispersion (35 Å/mm) spectra at $R = \lambda/\Delta\lambda = 2000$ inverse resolution (namely some 2.5 Å FWHM) in the wavelength range between 4600 and 5500 Å. Full details of the observing setup as well as of the data reduction can be found in Paper I.

A total of 100 stars had two or more observations along different nights while 39 stars were observed only once. Typically, a pixel-to-pixel S/N ratio greater than 50 was achieved in the 250 ob-

¹Based on observations collected at the INAOE “G. Haro” Observatory, Cananea (Mexico)

served spectra.

Wavelength calibration eventually provided a $\pm 0.09 \text{ \AA}$ accuracy, while spectral energy distribution (SED) of stars was obtained within a $\pm 10\%$ relative flux level. Flux rebinning to a fixed $\Delta\lambda/\text{pixel}$ ratio was performed preserving the total number of pixels as in the original observations.

Multiple observations also allowed us an independent estimate of the internal uncertainty of the whole data set. They confirmed in particular a pixel-to-pixel photon noise better than ± 0.02 mag, in agreement with the observed S/N ratio, with the only relevant exception of star HD 36389, which had poorer observations and S/N = 6 (cf. Table 1 in Paper I). Repeated observations for each star were eventually co-added after calibration in order to obtain one mean spectrum for each object.

Table 1 reports a full summary of the observed stellar sample listing in columns (1)–(4) respectively the HD number, spectral type, number of collected spectra, and mean flux uncertainty as from the standard deviation of the relative flux for repeated observations.²

2.1. Matching the Lick system

Three striking features of Fe I and the atomic-molecular blend of Mg I and MgH are present in the wavelength range of our spectra.

Each of these features has been included in the narrow-band spectral indices of the Lick system (Faber *et al.* 1977), in its recent extension by W94. A measure of the line strength is provided in this system by interpolating a local continuum (f_c) from two side bands adjacent to each relevant feature, and evaluating therefrom a pseudo-equivalent width ($E.W.$) such as

$$\begin{aligned} E.W. &= \int [(f_c(\lambda) - f(\lambda))/f_c(\lambda)] d\lambda \\ &= \Delta\lambda_f (1 - \langle f/f_c \rangle) \end{aligned} \quad (1)$$

where $\Delta\lambda_f$ is the width of the spectral window centered on the absorption feature.

For some molecular blends, it is useful to define

²For single observations, a mean $\sigma(\text{flux}) = 0.02$ will be assumed in this work.

an index in magnitude scale (I_{mag}) so that

$$\begin{aligned} I_{mag} &= -2.5 \log \left(\int [f(\lambda)/f_c(\lambda)] d\lambda / \Delta\lambda_f \right) \\ &= -2.5 \log \langle f/f_c \rangle \end{aligned} \quad (2)$$

Both formalisms are however equivalent (cf. also Brodie and Huchra 1990) as

$$E.W. = \Delta\lambda_f (1 - 10^{-0.4 I_{mag}}). \quad (3)$$

For each star in our sample, the Lick indices of Fe50, Fe52, Fe53, Mg₂ and Mgb have been computed in the instrumental system, following W94.

To account for the different spectral resolution of our observations, calibration to the standard system has been accomplished by matching the index calibrators in common with W94, B92 and B94, using the latter ones as a “check sample” in our fit.

We especially restrained our analysis to stars of class V-IV-III since class I-II supergiants are often variable stars and are therefore less confident calibrators.

A total of 36 stars were found in common with W94, with all available indices,³ while 13 secondary calibrators appeared in the B92 and B94 sample with standard Mg₂, Fe52 and Fe53 index measurements.

A zero-average (O–C) residual distribution (in the sense [Observed – Standard]) was eventually obtained with the following set of transformation equations:

$$\begin{aligned} (O - C)_{Fe50} &= 0.139 \text{ Fe50} - 0.278 & [\text{\AA}] \\ (O - C)_{Mg_2} &= -0.056 \text{ Mg}_2 + 0.007 & [\text{mag}] \\ (O - C)_{Mgb} &= 0.047 \text{ Mgb} - 0.092 & [\text{\AA}] \\ (O - C)_{Fe52} &= 0.150 \text{ Fe52} - 0.183 & [\text{\AA}] \\ (O - C)_{Fe53} &= 0.163 \text{ Fe53} + 0.078 & [\text{\AA}] \end{aligned} \quad (4)$$

In the equations, the input indices are the observed ones (that is in the instrumental system). After calibration, the residual standard deviation for the W94 primary calibrators and the B92/B94 “check sample”, resulted

$$\begin{aligned} \sigma(Fe50) &= \pm 0.39 \text{ \AA} & 35 \text{ stars} \\ \sigma(Mg_2) &= \pm 0.012 \text{ mag} & 49 \text{ stars} \\ \sigma(Mgb) &= \pm 0.19 \text{ \AA} & 36 \text{ stars} \\ \sigma(Fe52) &= \pm 0.24 \text{ \AA} & 49 \text{ stars} \\ \sigma(Fe53) &= \pm 0.25 \text{ \AA} & 49 \text{ stars.} \end{aligned} \quad (5)$$

³Apart from HD 49161, that lacks Fe50 in the W94 sample.

Figure 1 summarizes our results while the complete list of standard indices is reported in columns (5)–(9) of Table 1. When available from Paper I, column (10) provides the fiducial metallicity, while column (11) marks the reference calibrators in common with W94, B92 and B94.

A convenient estimate of the internal uncertainty of the whole data sample can easily derive from the typical pixel-to-pixel S/N ratio, recalling that $\sigma(\text{flux}) = (S/N)^{-1}$ mag. For each index, therefore, in a magnitude scale we could write

$$\sigma_I = \frac{\sigma(\text{flux})}{\sqrt{N_{red} + N_{blue} + N_{feat}}} \quad [\text{mag}] \quad (6)$$

where N_{red} , N_{blue} and N_{feat} are the number of pixels in the red and blue continuum side bands, and in the feature window, respectively. To translate from magnitudes to \AA equivalent width, we simply have

$$\sigma \text{ [\AA]} = \sigma \text{ [mag]} \times \Delta\lambda_f. \quad (7)$$

The typical internal error bar of our data eventually resulted in

$$\begin{aligned} \sigma(Fe50) &= \pm 0.32 \text{ \AA} \\ \sigma(Mg_2) &= \pm 0.004 \text{ mag} \\ \sigma(Mgb) &= \pm 0.19 \text{ \AA} \\ \sigma(Fe52) &= \pm 0.19 \text{ \AA} \\ \sigma(Fe53) &= \pm 0.22 \text{ \AA}. \end{aligned} \quad (8)$$

Note that the latter quantities consistently compare with the point scatter of eq. (5). This confirms that no residual variance was left in the data after transformation to the standard system via eq. (4).

3. The fiducial synthetic spectra

For 73 of the stars in Table 1 (nearly all those of luminosity classes V–III), we identified in Paper I a best choice for the atmosphere fundamental parameters available from high-resolution studies in the literature. In the following, this will be referred to as a “fair” sample. A further subsample of 18 stars had a formal atmosphere solution in our work, but with lower statistical confidence. The total of 91 stars will compose our “extended” sample.

Operationally, in Paper I our strategy was to compute, for each high-resolution parameter set,

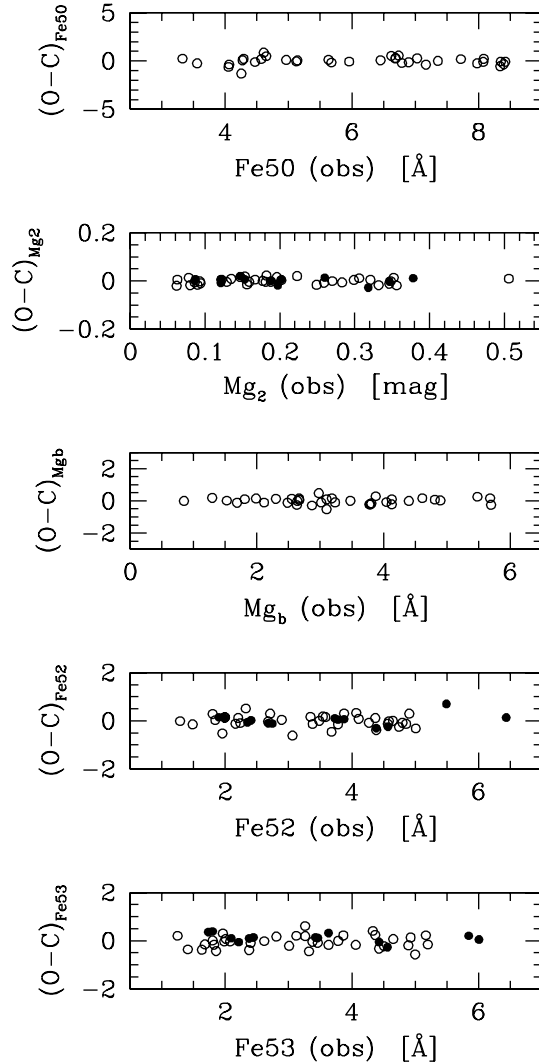


Fig. 1.— Index calibration to the standard Lick system. Residuals for the 36 primary calibrators (of luminosity class V–IV–III) in common with W94 (\circ) and a “check sample” of 13 stars in common with B92 and B94 (\bullet) are displayed, after application of eq. (4). Point scatter is $\sigma(Fe50) = \pm 0.39 \text{ \AA}$, $\sigma(Mg_2) = \pm 0.012 \text{ mag}$, $\sigma(Mgb) = \pm 0.19 \text{ \AA}$, $\sigma(Fe52) = \pm 0.24 \text{ \AA}$, and $\sigma(Fe53) = \pm 0.25 \text{ \AA}$. These values are comparable with the internal uncertainty in the observations confirming the reliability of the calibration procedure.

the corresponding synthetic spectrum from the Chavez *et al.* (1997) database and pick up the better fit to our mid-resolution spectra. This procedure allowed us to assess physical self-consistency of the high-resolution outputs and provide the best values for $\log T_{eff}$, $\log g$ and $[\text{Fe}/\text{H}]$.

In our analysis we had to face of course some intervening limitations of the Chavez *et al.* (1997) database, based on Kurucz (1993) models, at lower temperature and gravity. While, from one hand, the plane-parallel layer approximation is no longer valid in the model atmosphere for low-gravity stars ($\log g < 1.5$ dex), the incomplete sampling of the molecular contribution leads, on the other hand, to a poor representation of the SED in case of stars cooler than 4000 K.

In addition, when dealing with mid-resolution spectra, a study of our synthetic spectra showed that some unavoidable degeneracy in the allowed range of the atmosphere physical parameters is present, and statistically equivalent best fits to the observations may be provided by theoretical spectra with slightly different combinations of the distinctive parameters.

For example, we verified that the effect of any change in the effective temperature of a star can be compensated by a combined change of gravity and metallicity such as

$$\Delta \log g / \Delta T_{eff} = 1.3 (1000/T_{eff})^4 \text{ dex K}^{-1}, \quad (9)$$

and

$$\Delta[\text{Fe}/\text{H}] / \Delta T_{eff} = 7 \cdot 10^{-4} \text{ dex K}^{-1}. \quad (10)$$

Therefore, a warmer fitting temperature would accordingly imply a higher surface gravity and metallicity.

The $[\text{Fe}/\text{H}]$ vs. T_{eff} dependence even more magnifies in case we set gravity in the fitting synthetic spectra. Our tests show that

$$\Delta[\text{Fe}/\text{H}] / \Delta T_{eff} = 0.2 (1000/T_{eff})^3 \text{ dex K}^{-1}. \quad (11)$$

On the other hand, an opposite trend would result between gravity and metallicity in case we could fix the fitting temperature:

$$\Delta[\text{Fe}/\text{H}] / \Delta \log g = -0.35 \quad (12)$$

that is a higher metal abundance is required to balance “too shallower” absorption features in a spectrum in case of a lower surface gravity.

While therefore our mid-resolution observations alone prevented a univocal fit to the data, they allowed, though, to discriminate among different high-resolution parameter sets, and single out the best one for each star.

A total of 64 out of 91 stars in the “extended” sample resulted to be consistent with a metal abundance $[\text{Fe}/\text{H}] \geq 0.1$ dex suggesting that about 2/3 of the whole sample of 139 stars are actually composed by *bona fide* SMR stars.

As for the observed spectra, narrow-band spectral indices have been computed also for the corresponding set of synthetic spectra, and transformed to the Lick system by means of the empirical calibration of eq. (4).

In Fig. 2 we report the final residuals for the corresponding subsample of index calibrators with available fiducial model (the (O–C) residual distribution is now in the sense [Synthetic – Standard]). This consists of 25 primary reference stars in the W94 sample and 9 stars from the B92 and B94 list.

Point scatter in Fig. 2 is slightly higher compared with the observations (especially for the Magnesium indices and Fe50). This can be regarded as a measure of the “internal uncertainty” in the theoretical models due to the intrinsic limitation of the input physics:

$$\begin{aligned} \sigma(\text{Fe}50) &= \pm 0.70 \text{ \AA} & 25 \text{ stars} \\ \sigma(\text{Mg}_2) &= \pm 0.029 \text{ mag} & 34 \text{ stars} \\ \sigma(\text{Mgb}) &= \pm 0.40 \text{ \AA} & 25 \text{ stars} \\ \sigma(\text{Fe}52) &= \pm 0.27 \text{ \AA} & 34 \text{ stars} \\ \sigma(\text{Fe}53) &= \pm 0.34 \text{ \AA} & 34 \text{ stars.} \end{aligned} \quad (13)$$

3.1. Index calibration and atmosphere parameters

A more direct hint of the accuracy of the atmosphere fundamental parameters, at least for the 91 stars in our “extended sample”, can be done by comparing the (O–C) distribution (in the sense [Observed – Synthetic]) vs. fiducial set of temperature, gravity and metallicity. We especially focussed on the Mg_2 index and the “combined” Fe index defined as $\langle \text{Fe} \rangle = (\text{Fe}52 + \text{Fe}53)/2$ (Faber *et al.* 1985).

The (O–C) trend vs. surface gravity and temperature parameter $\Theta = 5040/T_{eff}$ is studied in Fig. 3. While a better match is achieved for the “fair sample” (solid dots), an increasing fraction of

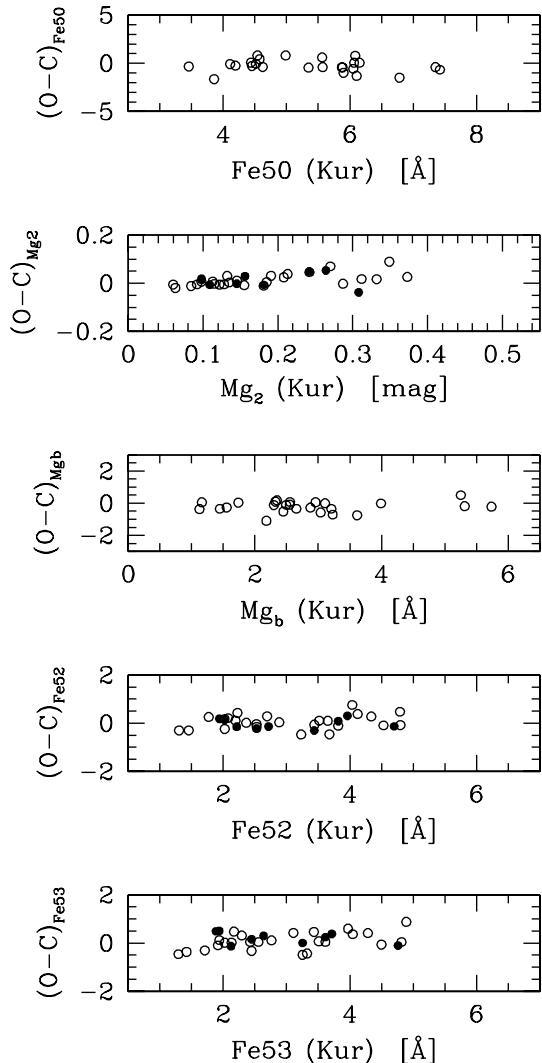


Fig. 2.— Index calibration to the standard Lick system, after eq. (4), for the fiducial model atmospheres of the 25 primary calibrators in common with W94 (\circ) and the 9 stars from B92 and B94 (\bullet). The (O–C) residuals are in the sense [Synthetic – Standard]. Point scatter is $\sigma(Fe50) = \pm 0.70 \text{ \AA}$, $\sigma(Mg_2) = \pm 0.029 \text{ mag}$, $\sigma(Mgb) = \pm 0.40 \text{ \AA}$, $\sigma(Fe52) = \pm 0.27 \text{ \AA}$, and $\sigma(Fe53) = \pm 0.34 \text{ \AA}$. These higher values, compared with those of the observations (cf. Fig. 1), give a measure of the residual variance of the theoretical models due to the intrinsic limitation of the input physics.

deviating points appears among cool (super)-giant stars (cf. open-dot distribution).

Both in the Mg_2 and $\langle Fe \rangle$ plots, four outliers, namely stars HD 36389 (sp. type M2Iab), HD 88230 (K8V), HD 146051 (M0.5III), and HD 157881 (K7V), display a very negative (O–C). These are the four coolest stars in our sample with $T_{eff} \leq 4000 \text{ K}$. As discussed in B92 and Chavez *et al.* (1996), most of this discrepancy arises from poor knowledge of molecular line opacities at cooler temperatures. This makes the atmosphere pseudocontinuum at 5000–5300 \AA higher, and the relevant indices stronger. These four stars will be excluded from further analyses, and we are therefore left with 72 stars for the “fair” sample and 87 stars for the “extended” sample.

According to the fiducial atmosphere parameters of Paper I, the resulting metallicity scale is explored in Fig. 4. As for Fig. 3, the (O–C) distribution vs. [Fe/H] does not show any significant trend being consistent in any case with a zero average. At least 6 stars can be confidently recognized on the plot with a metallicity in excess of [Fe/H] $> +0.35$ dex. Some of these SMR candidates have been discussed in detail in Paper I.

3.2. Magnesium vs. Iron relative abundance

A study of the Mg_2 and $\langle Fe \rangle$ residuals could also provide important information about the Mg vs. Fe relative abundance. As Kurucz model atmospheres and Chavez *et al.* (1997) synthetic spectra assume a solar chemical partition (so that [Mg/Fe] = 0.0, by definition), any systematic deviation in the index residuals could therefore track, on the average, a non-standard chemical mix for real stars.

Two opposite trends in the (O–C) distribution might be envisaged, in this respect, depending whether they are induced by a biased set of atmosphere parameters or rather by a non-solar abundance partition for [Mg/Fe]. In the first case, a mismatch of either T_{eff} and/or $\log g$ would reflect in a nominal metallicity shift (in force of eqs. (10)–(12), and therefore in a *correlated* trend of Mg_2 and $\langle Fe \rangle$ (O–C) residuals. On the contrary, any *intrinsic* change of the [Mg/Fe] relative abundance would induce *anti-correlated* (O–C)s for the two indices.

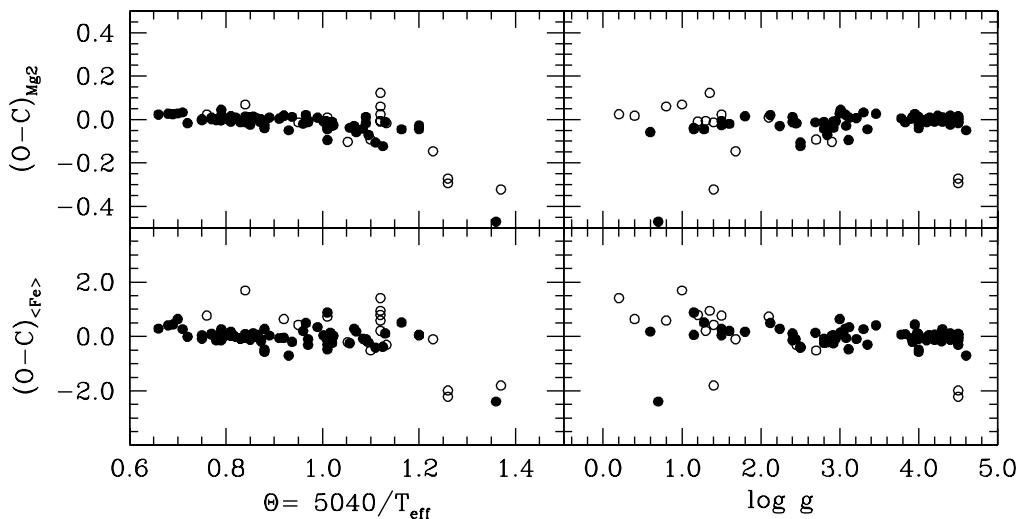


Fig. 3.— The $(O-C)$ index residuals (in the sense [Observed – Synthetic]) for Mg_2 and combined Iron index $\langle Fe \rangle$ are displayed vs. atmosphere fiducial parameters $\Theta = 5040/T_{eff}$ and surface gravity. Solid dots mark the “fair sample” of 73 stars while open dots include the supplementary 18 stars with less confident atmosphere match. As expected, the four coolest stars in the sample ($T_{eff} \leq 4000$ K) are poorly matched by the models while the remaining point distribution is consistent with a zero-average residual. These four outliers will not enter any further analysis.

As far as the the “fair” sample is accounted for in our analysis (cf. solid dots distribution in Fig. 5) no statistically significant trend between Mg and Fe indices is evident within a $2\text{-}\sigma$ confidence level. As expected, most of the deviating points in the figure belong to the “extended” sample, and the correlated distribution in the latter case is therefore induced as a result of the less accurate atmosphere fit.

In conclusion, we have therefore no evident sign of a systematic trend in the $[Mg/Fe]$ relative abundance, and a standard chemical partition seems consistent with the data.

4. Comparison with index fitting functions

Lick narrow-band indices have proven to be an useful diagnostic tool not only to probe atmosphere physical properties in individual stars but also for studying stellar populations as a whole (Buzzoni 1995, 1996; Worthey *et al.* 1992, 1996).

In particular, population synthesis models have made extensive use of the “fitting function” tech-

nique to compute integrated indices for theoretical stellar systems.

This procedure relies on analytical fits of the index strength vs. stellar fundamental parameters (namely $\log T_{eff}$, $\log g$, and $[Fe/H]$) across the H-R diagram, and allows spectroscopic features to be synthesized for stellar aggregates even by means of low-resolution models of the integrated SED.

For example, if an index I can be defined for individual stars in a magnitude scale like in eq. (2), then by summing up on the whole stellar population, we have

$$I_{tot} = -2.5 \log \left(\frac{\sum_* f_c(i) \times 10^{-0.4 I(i)}}{\sum_* f_c(i)} \right). \quad (14)$$

If the dex term in the r.h. upper sum can be evaluated analytically for each composing star, then the integrated index simply follows in terms of the total continuum luminosity of the whole population, $L_{tot} = \sum_* f_c(i)$ (see B92 for a first application of this technique to the Mg_2 synthesis).

Analytical fitting functions for Iron and Magnesium indices have been provided by B92, B94 and

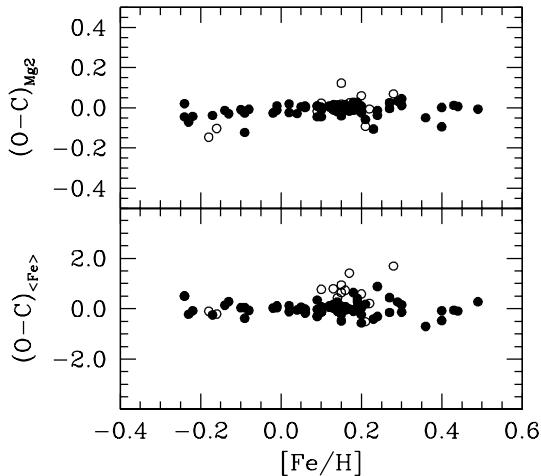


Fig. 4.— The metallicity scale is explored vs. (O–C) index residuals (in the sense [Observed – synthetic]) like in Fig. 3. No (O–C) trend is found vs. [Fe/H], with index residual distribution consistent with a zero average. At least 6 stars can be confidently recognized with [Fe/H] in excess of +0.35 dex.

Gorgas *et al.* (1993). The latter set of equations has then been revised by W94 including a larger number of features in the optical wavelength range and calibrating vs. effective temperature.

It could be useful to test self-consistency of these functions also in the SMR regime in order to secure their application to the synthesis of metal-rich stellar environments, like in the case of the Galaxy bulge or external early-type galaxies.

A first check in this sense can be done by studying the index residuals of our observations both with respect to the B92, B94 and W94 sets of fitting functions. Figure 6 summarizes our results for Mg_2 .

Both (O–C) distributions in the figure are consistent with a zero average residual confirming that the two sets of equations properly account for high-metallicity stars. The W94 fitting function is slightly more accurate than the B92 one (point spread for the “fair sample” is $\sigma(Mg_2) = \pm 0.031$ mag vs. $\sigma(Mg_2) = \pm 0.049$ mag for the latter case), but at cost of a more elaborated analytical fit consisting of four different polynomials

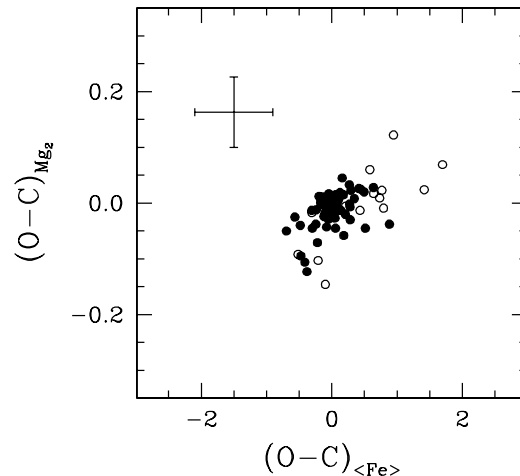


Fig. 5.— The Mg_2 and $\langle Fe \rangle$ index residuals between observations and fiducial synthetic spectra are displayed for the “fair” (\bullet) and the “extended” (\circ) sample. The typical $2\text{-}\sigma$ error box of individual observations is displayed top left in the figure. The lack of any clear *anti-correlated* trend between the (O–C) residuals indicates, on the average, a solar [Mg/Fe] relative abundance. See text for discussion.

along the temperature range of stars.⁴

A similar behaviour is also found for the $\langle Fe \rangle$ index (cf. Fig. 7) with $\sigma(\langle Fe \rangle) = \pm 0.61 \text{ \AA}$ with respect to B94, and $\sigma(\langle Fe \rangle) = \pm 0.30 \text{ \AA}$ with respect to the W94 three-branch fit. We verified that the skewed positive residuals with respect to B94, evident from the figure, mostly come from the warmer stars in the sample ($T_{eff} \gtrsim 6700 \text{ K}$) for which the fitting function predicts a vanishing Fe52 index.

The Fe50 and Mgb features have been accounted only by W94. Fitting function predictions are compared with observations in Fig. 8. Data seem more poorly matched, compared with Mg_2 and $\langle Fe \rangle$, with a more important (O–C) spread ($\sigma(Fe50) = \pm 0.95 \text{ \AA}$, and $\sigma(Mgb) = \pm 0.83 \text{ \AA}$ for

⁴Quite importantly, note that an incorrect version of one of the four polynomial branches is given in the Worthey *et al.* (1994) Table 3. The claimed $\log \Theta$ dependence of the fit should in fact be read as a simple Θ dependence. The same problem affects also all the other indices discussed in this work.

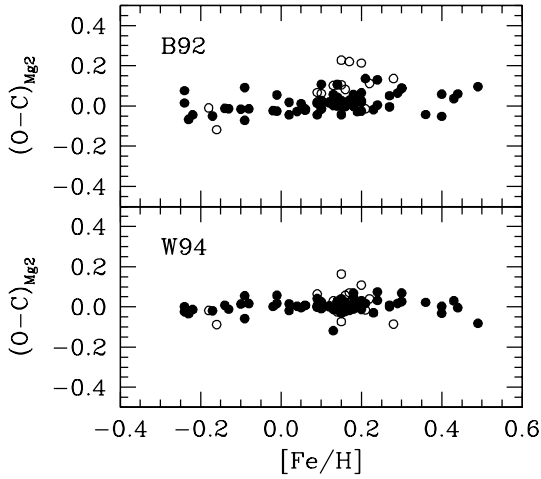


Fig. 6.— The Mg_2 index residuals (in the sense [Observed – Computed]) with respect to B92 and W94 fitting functions vs. metallicity for the “fair” (\bullet) and the “extended” (\circ) samples. Both (O–C) distributions are consistent with a zero average. Point spread for the “fair” sample across the B92 fitting function is $\sigma(Mg_2) = \pm 0.049$ mag, and $\sigma(Mg_2) = \pm 0.031$ mag with respect to W94.

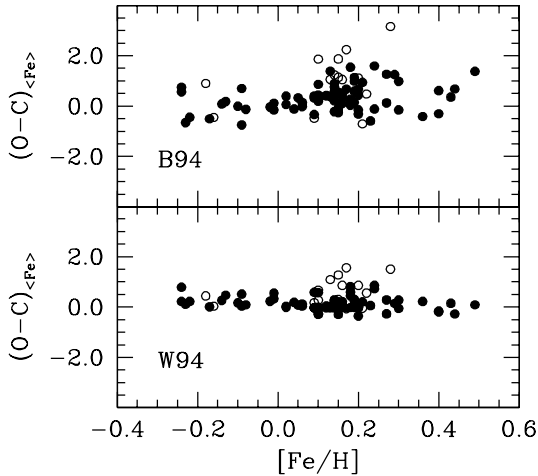


Fig. 7.— Same as for Fig. 6 but for the combined Fe index $\langle Fe \rangle = (Fe_{52} + Fe_{53})/2$. Point spread of the “fair sample” (\bullet) with respect to the zero-average (O–C) is $\sigma(\langle Fe \rangle) = \pm 0.61$ Å comparing with B94, and $\sigma(\langle Fe \rangle) = \pm 0.30$ Å with respect to W94.

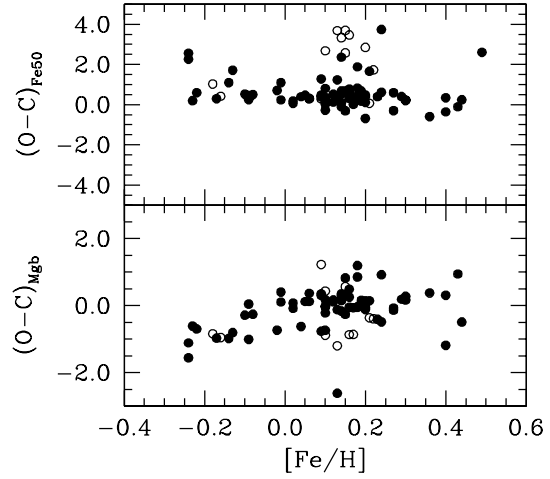


Fig. 8.— Same as for Fig. 6 but for the Fe50 and Mgb indices. The (O–C) residuals are computed with respect to the W94 fitting functions. Point spread for the “fair sample” (\bullet) with respect to the zero-average (O–C) is $\sigma(Fe_{50}) = \pm 0.95$ Å, and $\sigma(Mgb) = \pm 0.83$ Å. A trend with $[Fe/H]$ (opposite for Fe50 and Mgb) appears in the data.

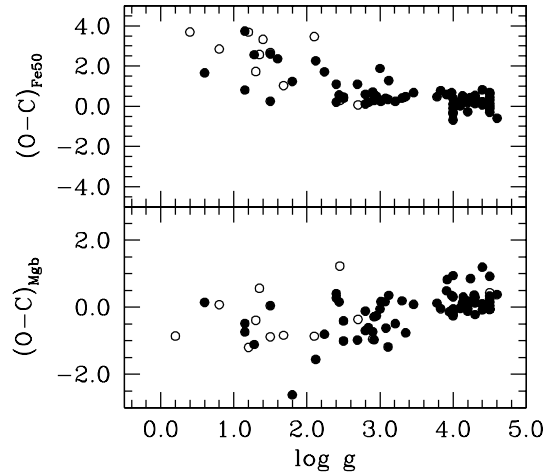


Fig. 9.— The Fe50 and Mgb (O–C) residuals as from Fig. 8 is explored vs. stellar gravity. The drift in the data distribution indicates that $\log g$ dependence is not fully accounted for by the W94 fitting functions. The residual variance is the main responsible for the poorer match to the observations in Fig. 8.

the “fair sample”), and a non-zero (O–C) average.

If we explore the (O–C) distribution vs. stellar surface gravity (cf. Fig. 9) the drift of the data is even increased confirming that $\log g$ dependence has not been fully accounted for by the W94 fitting functions. This residual variance is expected to induce a biased measure of the integrated Fe50 and Mgb as far as population synthesis models are computed relying on the W94 theoretical framework. Special caution should therefore be recommended in the synthesis of these indices.

4.1. Fitting functions and index fit

Although each of the B92, B94 and W94 fitting functions assures a convenient representation of the Mg_2 and $\langle Fe \rangle$ indices in the metallicity range of our observations, it is however worth to briefly discuss here a possible important bias dealing with any unwarranted use of the fitting function technique to reproduce stellar indices.

The problem could be of paramount importance in case of population synthesis models, where fitting functions are used to a systematic prediction of index behaviour across the whole H-R diagram and often beyond the boundary limits of the formal fitting domain.

An instructive example in this sense is given in Fig. 10, where we compare Mg_2 distribution of our stellar sample with the B92 and W94 analytical output. In order to span the whole range of temperature, to our stars we also added the Mg_2 measurements of eight Gliese red dwarfs from B92 in both panels) and ten M dwarfs from the Gorgas *et al.* (1993) sample with $3000 < T_{eff} < 4300$ K, according to the $(V - K)$ vs. T_{eff} calibration of W94 (cf. Table 6 therein). A set of 16 field M giants with $T_{eff} < 3900$ K, from Table A2C of W94, is also included in the figure to span low-gravity stars.

To ease comparison, our observations have been corrected for metallicity and reconducted to $[Fe/H] = 0$ by subtracting the $[Fe/H]$ polynomial term according to the different fitting sets. In each panel of the figure, three theoretical loci are computed for $\log g = 5.0, 2.0$ and -1.0 dex at solar metallicity.

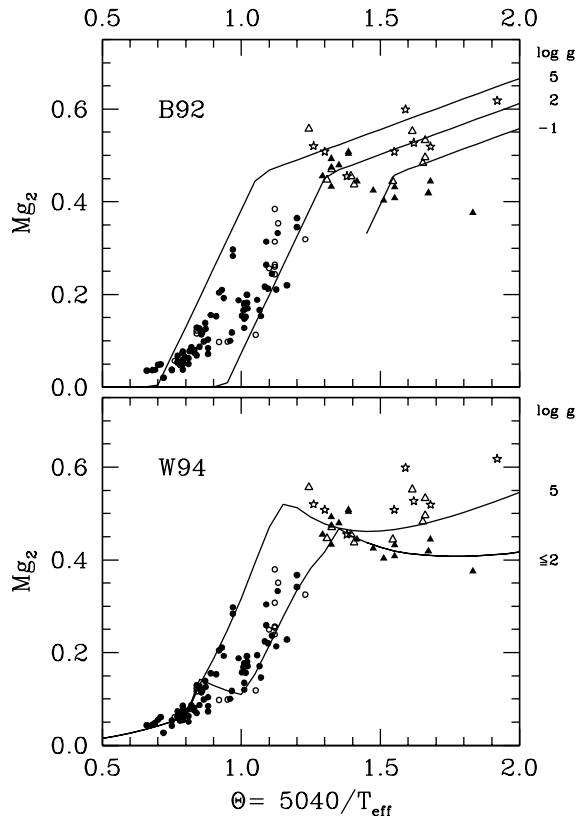


Fig. 10.— The Mg_2 data distribution (\bullet = “fair”, \circ = “extended” samples) vs. B92 and W94 fitting function predictions (solid lines). To ease comparison, observations have been corrected to $[Fe/H] = 0$ by subtracting the corresponding $[Fe/H]$ polynomial term of each fitting set. In order to span the whole range of temperature, also Mg_2 measurements of eight Gliese red dwarfs from B92 (“ \star ” markers) have been added in both panels together with ten M dwarfs from the Gorgas *et al.* (1993) sample (“ Δ ”). The low-gravity range is also spanned by a set of 16 field M giants with $T_{eff} < 3900$ K, from W94 (“ \blacktriangle ”). The B92 and W94 fitting functions have been computed for $\log g = 5.0, 2.0$ and -1.0 dex, as labelled in each panel. Below 3900 K the W94 fit is insensitive to stellar gravity so that the $\log g = 2$ and -1 curves merge. A solar metallicity is assumed throughout in the models.

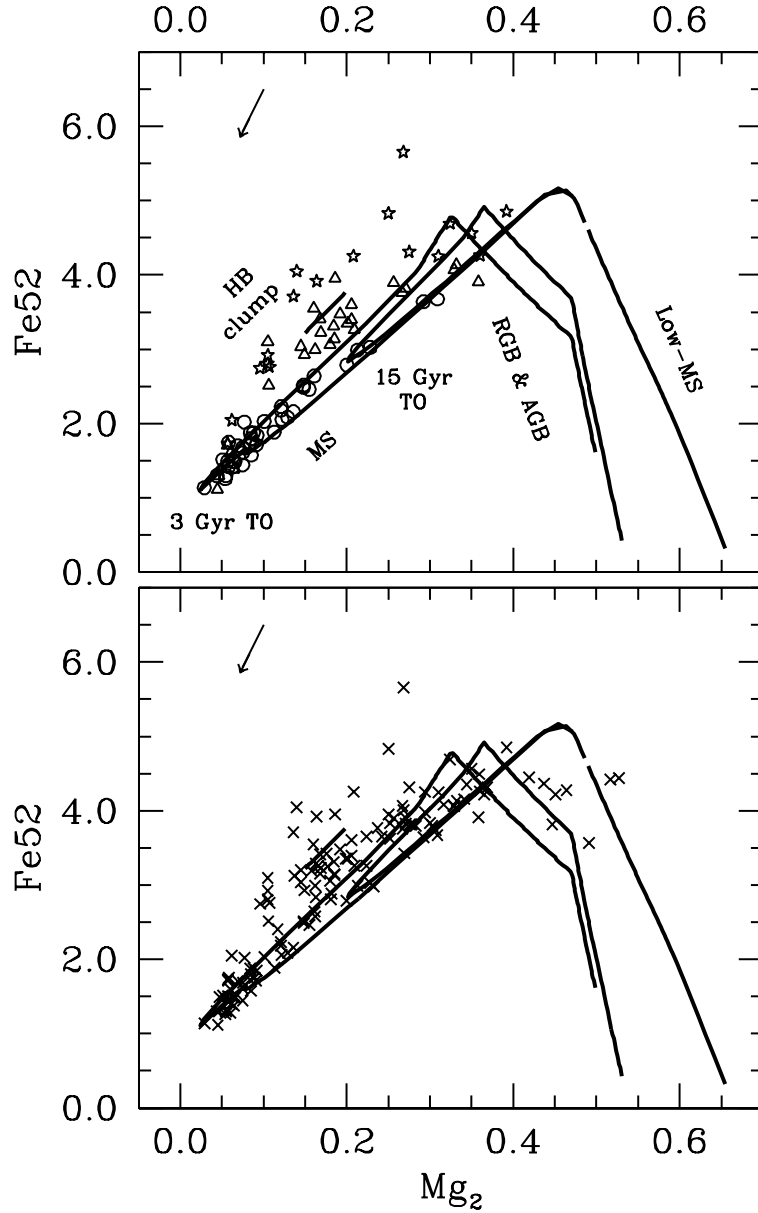


Fig. 11.— The Mg_2 vs. Fe52 distribution for the 87 stars with fiducial atmosphere parameters in the “extended” sample (*upper panel*) and for the global observed sample of 139 stars (*lower panel*). Stars in the upper panel are marked according to their surface gravity (\star : $\log g < 2.0$; Δ : $2.00 \leq \log g \leq 3.5$; \circ : $\log g > 3.5$). The theoretical locus for a 3 and 15 Gyr old simple stellar populations with $[Fe/H] = +0.2$ from Buzzoni (1989) is superposed to the data, and main evolutionary phases are labelled (MS = main sequence; TO = MS Turn off point; RGB = red giant branch; AGB = asymptotic giant branch; HB = horizontal branch). The vector top left in each panel is the expected variation in the observed indices for a change in $[Fe/H]$ of -0.5 dex.

TABLE 1
OBSERVATIONAL DATABASE AND STANDARD LICK INDICES

HD	Sp. Type	n(obs)	σ (flux)	Fe50 [Å]	Mg ₂ [mag]	Mg _b [Å]	Fe52 [Å]	Fe53 [Å]	[Fe/H] ^a	Remarks ^b
4	F0	1	...	4.098	0.075	1.447	1.682	1.269	+0.3	
1461	G0V	2	0.0048	4.552	0.148	3.175	2.487	1.932	+0.43	W
1835	G3V	2	0.0109	4.722	0.148	3.019	2.515	1.968	+0.19	B
4188	K0III	3	0.0068	5.952	0.105	2.548	3.096	2.491	-0.16	
6497	K2III	3	0.0061	6.294	0.307	4.131	3.736	3.351	...	
8673	F7V	2	0.0037	3.754	0.085	1.505	1.574	1.233	+0.16	
10307	G1.5V	3	0.0068	3.766	0.136	2.610	2.160	1.565	-0.02	W
10780	K0V	2	0.0046	4.690	0.228	4.677	3.026	2.441	+0.36	W
15152	K5III	2	0.0095	7.602	0.437	4.389	4.366	4.385	...	
16232	F6V	2	0.0051	3.284	0.062	1.119	1.408	0.984	+0.27	
17017	K2III	2	0.0076	6.399	0.252	3.513	3.621	3.149	...	
18322	K1III	2	0.0056	5.838	0.201	3.197	3.353	2.788	-0.23	B
19476	K0III	4	0.0068	6.080	0.184	2.826	3.312	2.749	+0.04	W
20630	G5V	2	0.0080	4.245	0.155	3.049	2.460	1.912	-0.01	W B
20675	F6V	3	0.0047	3.725	0.065	1.079	1.485	1.170	+0.2	
21488	K0	4	0.0159	5.023	0.162	2.164	2.574	2.276	...	
24240	K0III	3	0.0065	6.730	0.176	2.597	3.423	2.894	...	
24802	K0	3	0.0081	7.159	0.250	2.782	3.949	3.396	...	
25975	K1III	3	0.0052	5.416	0.224	3.772	3.261	2.681	...	
26462	F4V	3	0.0016	3.142	0.060	0.901	1.278	0.965	...	W
26846	K3III	2	0.0041	6.741	0.267	3.843	3.758	3.352	+0.21	
27371	K0III	3	0.0060	6.333	0.169	2.459	3.228	2.703	-0.02	W
27697	K0I	3	0.0017	6.349	0.177	2.434	3.251	2.699	...	W
28307	K0IIIb	3	0.0019	6.124	0.185	2.637	3.148	2.654	...	W
30495	G3V	2	0.0026	3.932	0.121	2.857	2.181	1.676	+0.1	B
30562	F8V	2	0.0032	4.708	0.121	2.390	2.229	1.774	+0.14	B
30652	F6V	3	0.0039	3.341	0.075	1.326	1.445	1.101	+0.02	W
32068	K4Ib-II+...	2	0.0101	8.411	0.350	3.018	4.563	4.453	+0.1	
32393	K3	1	...	7.057	0.328	4.093	4.063	3.702	...	
33276	F2IV	2	0.0076	3.342	0.064	0.989	1.381	1.116	+0.29	
34411	G1.5IV-V	2	0.0034	4.212	0.122	2.523	2.057	1.661	+0.06	W
35620	K3IIICN+...	1	...	7.232	0.360	3.721	4.262	4.046	-0.09	W
36040	K0IIIp	1	...	6.828	0.242	3.321	3.650	3.134	...	
36389	M2Iab	2	0.0066	7.183	0.232	2.889	2.977	3.005	+0.11	
37387	K1Ib	1	...	10.895	0.250	1.484	4.831	4.433	+0.13	
37763	K3III	1	...	7.135	0.329	4.119	4.068	3.742	+0.3	B
42341	K2III	1	...	7.144	0.294	4.154	3.980	3.670	...	
44391	K0Ib	2	0.0111	8.916	0.164	1.373	3.919	3.278	+0.21	
44478	M3II	2	0.0095	10.685	0.491	7.131	3.563	3.502	...	
45412	F8Ib var	2	0.0046	5.721	0.062	0.187	2.048	1.682	+0.1	
46709	K4III	2	0.0101	7.900	0.359	3.444	4.492	4.297	...	
47174	K3Iab:	2	0.0046	6.988	0.237	2.958	3.766	3.226	...	
48682	G0V	2	0.0083	3.972	0.092	2.106	1.845	1.475	+0.15	W
49161	K4III	2	0.0052	7.931	0.344	3.709	4.353	4.248	...	W
52973	G0Ib var	2	0.0078	7.722	0.096	0.258	2.745	2.083	+0.49	
54719	K2III	2	0.0071	7.511	0.267	3.405	4.065	3.577	...	W
56577	K4III	1	...	9.760	0.392	3.437	4.853	4.814	+0.15	B
57727	G8III	2	0.0045	5.175	0.163	2.536	2.833	2.189	...	
58207	G9IIIb	2	0.0064	5.832	0.180	2.600	3.057	2.534	-0.17	W

TABLE 1—*Continued*

HD	Sp. Type	n(obs)	σ (flux)	Fe50 [Å]	Mg ₂ [mag]	Mg _b [Å]	Fe52 [Å]	Fe53 [Å]	[Fe/H] ^a	Remarks ^b
59881	F0III	3	0.0077	2.642	0.045	0.727	1.115	0.864	+0.19	
60522	M0I	2	0.0331	5.268	0.451	5.010	4.220	2.926	...	W
61064	F6III	2	0.0107	4.308	0.060	0.761	1.602	1.259	+0.44	
62902	K5III	2	0.0091	7.668	0.419	4.766	4.445	4.531	...	
63302	K3Iab/Ib	1	...	13.493	0.268	0.804	5.656	4.952	+0.17	B
63700	G3Ib	1	...	10.381	0.140	0.341	4.049	3.527	+0.24	
65714	gG8	2	0.0100	6.773	0.163	2.299	3.288	2.735	...	
72184	K2III	2	0.0042	6.613	0.278	4.028	3.813	3.322	...	W
72324	G9I	2	0.0070	6.246	0.168	2.348	3.150	2.544	...	W
72505	K0III	2	0.0085	6.849	0.300	3.852	3.837	3.455	...	
72561	G5III	2	0.0068	6.801	0.145	1.573	3.203	2.583	...	
73665	K0I	2	0.0071	6.672	0.166	2.382	3.256	2.685	...	W
73710	K0I	2	0.0303	4.822	0.117	1.399	2.407	1.876	...	W
74739	G7.5IIIa	2	0.0117	6.479	0.145	1.722	3.038	2.454	-0.14	
75732	G8V	3	0.0059	5.980	0.309	5.522	3.674	3.089	+0.24	W
78249	K1IV	2	0.0121	5.558	0.269	4.354	3.427	2.841	...	
81029	F0	1	...	3.298	0.051	0.565	1.515	1.015	+0.27	
81873	K0III	2	0.0068	6.245	0.199	2.893	3.357	2.806	...	
82734	K0IV	1	...	6.718	0.168	2.412	3.411	2.908	+0.4	
83951	F3V	2	0.0045	3.130	0.044	0.853	1.299	0.975	+0.14	
85503	K0III	2	0.0080	7.532	0.332	4.286	4.135	3.817	-0.01	W
87822	F4V	2	0.0087	3.489	0.063	1.210	1.491	1.165	+0.19	
88230	K8V	2	0.0137	5.126	0.527	4.759	4.442	4.106	+0.28	W
88284	K0III	1	...	6.452	0.192	3.049	3.478	2.963	+0.09	W B
90277	F0V	2	0.0082	3.129	0.046	0.739	1.297	0.960	+0.19	
92125	G2.5IIa	2	0.0129	6.431	0.106	1.088	2.515	2.168	-0.24	
93257	gK3	2	0.0139	6.408	0.303	4.284	3.796	3.337	...	
95272	K0III	1	...	6.216	0.206	2.965	3.397	2.818	-0.22	W B
95849	K3III	2	0.0106	7.243	0.270	3.560	3.909	3.559	...	
100563	F5V	2	0.0087	3.488	0.066	1.418	1.489	1.203	+0.12	
101013	K0IIIp	1	...	5.099	0.181	1.888	2.809	1.980	...	
102328	K3III	2	0.0171	7.468	0.365	4.487	4.216	4.019	...	W
102634	F7V	2	0.0055	4.060	0.085	1.782	1.798	1.373	+0.1	B
102870	F9V	2	0.0044	4.127	0.084	1.814	1.876	1.429	+0.18	W B
104304	G9IV	2	0.0045	5.174	0.213	4.120	2.989	2.400	+0.18	
109511	K2III	2	0.0089	6.663	0.206	2.834	3.603	3.057	-0.09	
110014	K2III	1	...	7.518	0.294	3.617	4.252	3.769	...	
113022	F6Vs	1	...	3.576	0.057	1.432	1.500	1.109	+0.1	
114710	F9.5V	1	...	3.775	0.088	2.282	1.880	1.450	+0.02	W
115604	F3III	1	...	4.506	0.057	0.693	1.713	1.373	+0.18	
120136	F6IV	1	...	3.940	0.058	1.544	1.750	1.326	+0.14	W
121370	G0IV	1	...	4.704	0.077	1.700	2.022	1.585	+0.16	W
124425	F7IV	1	...	3.587	0.047	1.010	1.496	1.044	...	
124570	F6IV	1	...	3.952	0.069	1.517	1.702	1.325	+0.12	
125560	K3III	1	...	7.148	0.316	4.028	4.080	3.695	...	W
127227	K5III	1	...	7.608	0.464	4.680	4.275	4.491	...	
129989	K0II-III	1	...	7.623	0.160	2.054	3.549	3.004	-0.13	
130948	G1V	1	...	3.712	0.113	2.327	1.886	1.413	+0.2	
136028	K5I	1	...	4.126	0.341	4.093	4.156	2.102	...	W

TABLE 1—*Continued*

HD	Sp. Type	n(obs)	$\sigma(\text{flux})$	Fe50 [Å]	Mg ₂ [mag]	Mg _b [Å]	Fe52 [Å]	Fe53 [Å]	[Fe/H] ^a	Remarks ^b
139357	gK4	1	...	7.535	0.268	3.807	4.010	3.709	...	
140573	K2IIIb	1	...	7.236	0.256	3.693	3.898	3.548	+0.23	W
144284	F8IV	4	0.0063	4.098	0.075	1.447	1.682	1.269	+0.2	
145000	K1III	1	...	6.841	0.224	3.366	3.649	3.219	...	
145675	K0V	2	0.0101	6.036	0.292	5.508	3.640	3.158	+0.18	W
146051	M0.5III	2	0.0093	7.362	0.447	4.757	3.818	3.970	+0.32	
147677	K0III	1	...	6.039	0.158	2.633	3.195	2.651	...	W
148513	K4III	1	...	7.460	0.369	3.948	4.312	4.276	...	W
150680	G0IV	2	0.0055	4.390	0.101	2.022	2.030	1.636	-0.07	
153956	gK1	1	...	6.821	0.276	3.564	3.812	3.324	...	
156266	K2III	1	...	6.692	0.252	3.512	3.830	3.320	...	
156283	K3Iab:	2	0.0100	7.798	0.310	3.083	4.250	3.899	-0.18	
									...	
157881	K7V	2	0.0067	5.017	0.517	4.687	4.419	4.156	+0.4	
159181	G2Iab:	2	0.0075	7.377	0.107	0.735	2.763	2.394	+0.14	
159925	G9III	1	...	6.117	0.137	2.129	3.123	2.432	...	
160922	F5V	2	0.0091	3.211	0.058	1.323	1.423	1.054	+0.4	
161096	K2III	2	0.0146	7.130	0.271	3.866	3.824	3.494	+0.14	
161797	G5IV	3	0.0053	5.166	0.161	3.128	2.641	2.112	+0.16	W
162917	F4IV-V	4	0.0049	3.343	0.055	1.241	1.302	0.865	+0.1	
163770	K1IIaCN+...	1	...	9.177	0.208	1.748	4.253	3.827	-0.24	
163993	G8III	3	0.0056	5.796	0.149	2.498	2.928	2.342	-0.1	
166229	K2.5III	1	...	6.535	0.283	3.936	3.798	3.386	...	
167858	F2V	3	0.0067	2.805	0.029	0.792	1.137	0.826	+0.17	
171802	F5III	2	0.0032	2.949	0.054	1.151	1.259	0.772	+0.1	
181276	G9III	2	0.0055	5.863	0.162	2.696	2.990	2.284	-0.08	
182572	G8IV...	2	0.0040	5.408	0.200	3.788	2.787	2.271	+0.15	W
186408	G1V	2	0.0043	4.281	0.129	2.931	2.085	1.604	+0.06	W
187238	K3Ia0-Ia	3	0.0054	10.377	0.324	2.424	4.690	4.407	+0.2	
187299	G5Ia0-Ib	2	0.0054	9.634	0.186	1.179	3.954	3.374	+0.16	
187691	F8V	2	0.0037	3.958	0.091	1.987	1.714	1.285	+0.09	W
187921	G2.5:Iab	3	0.0101	10.689	0.136	-0.425	3.711	2.975	+0.28	
196725	K3Iab	2	0.0070	9.088	0.275	2.517	4.311	4.142	+0.22	
197039	F5	2	0.0034	3.926	0.075	1.465	1.607	1.164	+0.15	
197572	F7Ib...	3	0.0057	8.352	0.105	0.417	2.804	2.215	+0.15	
197963	F7V	1	...	5.464	0.182	3.030	2.886	2.516	...	
198084	F8IV-V	2	0.0032	4.106	0.084	1.739	1.727	1.388	+0.12	
201078	F7.5Ib-IIvar	2	0.0039	4.803	0.057	0.406	1.735	1.203	+0.13	
205512	K0.5III	2	0.0050	6.232	0.209	3.091	3.262	2.793	+0.2	
209750	G2Ib	2	0.0049	8.247	0.105	0.531	2.920	2.462	+0.14	
216228	K0III	2	0.0041	6.104	0.185	2.908	3.136	2.626	+0.09	
221148	K3IIIvar	2	0.0059	6.925	0.358	5.316	3.909	3.628	+0.09	W B

^aFrom Paper I^bIndex calibrator in common with Worthey et al. (1994) [W] or Buzzoni et al. (1992, 1994) [B]

While both fitting sets properly comprise our data distribution (thus confirming the adequacy of the fit, as we discussed in previous section), it is however evident that a different trend for the Mg_2 index is predicted at low temperature.

Compared with W94, for $\Theta \gtrsim 1.3$ ($T_{eff} \lesssim 3900$ K) the B92 fitting function shows a steeper increase in the Mg index. This better matches the red-dwarf data, although some marginal evidence exists for an overestimate of the M giants. On the other hand, the W94 fit predicts slightly lower values for Mg_2 throughout in the low-temperature range, and partially misses the red-dwarf data. Moreover, an artificial glitch is evident in one of the fitting branches of the W94 set at about $\Theta = 0.8 - 1.0$ for $\log g = 2$.

Such a different behaviour in the H-R diagram description directly reflects in the theoretical output when computing integrated indices for population synthesis models. This explain, for instance, the systematically lower values for Mg_2 in the Worthey (1994) simple stellar population models compared with B92.

5. The Mg_2 vs. Fe52 diagnostics

Given a selective dependence on the atmosphere fundamental parameters, a combined study of the Mg and Fe Lick indices could give direct hints on the distinctive parameters of stars.

A two-index plot, like in Fig. 11, summarizes in facts most of the relevant features of a c-m diagram but with a major advantage to be both reddening free and distance independent, and points therefore to the intrinsic properties of stars.

In the upper panel of the figure we study the “fair sample” distribution in the Mg_2 vs. Fe52 index domain with two $[Fe/H] = +0.22$ dex isochrones of 3 and 15 Gyr from the Buzzoni (1989) synthesis code. Surface gravity of stars in our sample has been singled out for a better comparison with the models, while the main evolutionary phases for both isochrones have been labelled on the plot.

A quite good agreement exists between high-gravity stars ($\log g > 3.5$ dex) and the main sequence locus confirming that objects as young as 3 Gyr are present in our sample. This makes a $Mg_2/Fe52$ plot a simple and very powerful tool to estimate age of stellar populations.

Stars of intermediate gravity ($2.0 \geq \log g \geq 3.5$) consistently “bunch” around the expected locus for the core Helium-burning stars (both the horizontal branch phase of low-mass stars or the first blue loop of high-mass objects) while a lack of objects close to the tip of the red- and asymptotic giant branches (that is for a vanishing value of Fe52 with $Mg_2 \gtrsim 0.4$ in the plot) seem to indicate a prevailing presence in our sample of high-mass stars ($M > 2M_{\odot}$) developing a non-He-degenerate red giant phase.

It is a pleasure to thank Guy Worthey, the referee of this paper, for his valuable input and important suggestions. This project received partial financial support from the Italian MURST under COFIN’98 02-013, COFIN’00 02-016 and 60% grants, and from the Mexican CONACyT via grant 28506-E.

REFERENCES

- Brodie, J. P., and Huchra, J. P. 1990, *ApJ*, 362, 503
- Buzzoni, A. 1989, *ApJS*, 71, 817
- Buzzoni, A. 1995, *ApJS*, 98, 69
- Buzzoni, A. 1996 in *Fresh Views of Elliptical Galaxies*, ed. A. Buzzoni, A. Renzini and A. Serrano (San Francisco: ASP) p. 189
- Buzzoni, A., Gariboldi, G., and Mantegazza, L. 1992, *AJ*, 103, 1814 (B92)
- Buzzoni, A., Mantegazza, L., and Gariboldi, G. 1994, *AJ*, 107, 513 (B94)
- Cayrel de Strobel, G., Soubiran, C., Friel, E. D., Ralite, N., and François, P. 1997, *A&AS*, 124, 299
- Chavez, M., Malagnini, M. L., and Morossi, C. 1996, *ApJ*, 471, 726
- Chavez, M., Malagnini, M. L., and Morossi, C. 1997, *A&AS*, 126, 267
- Faber, S. M., Burstein, D., and Dressler, A. 1977, *AJ*, 82, 941
- Faber, S. M., Friel, E. D., Burstein, D., and Gaskell, C. M. 1985, *ApJS*, 57, 711

- Frogel, J. A. 1999, *Ap&SS*, 265, 303
- Gorgas, J., Faber, S. M., Burstein, D., Gonzalez, J. J., Courteau, S., and Prosser, C. 1993, *ApJS*, 86, 153
- Kurucz, R. L. 1993, CD-ROM 13, ATLAS9 Stellar Atmosphere Programs and 2 km/s Grid (Cambridge: SAO)
- Malagnini, M. L., Morossi, C., Buzzoni, A., and Chavez, M. 2000, *PASP*, 112, 1455 (Paper I)
- McWilliam, A. 1997, *ARA&A*, 35, 503
- Smith, G., and Ruck, M. J. 2000, *A&A*, 356, 570
- Taylor, B. J. 1991, *ApJS*, 76, 715
- Taylor, B. J. 1999, *A&A*, 344, 655
- Worthey, G. 1994, *ApJS*, 95, 107
- Worthey, G., Faber, S. M., and Gonzalez, J. J. 1992, *ApJ*, 398, 69
- Worthey, G., Faber, S. M., Gonzalez, J. J., and Burstein, D. 1994, *ApJS*, 94, 687 (W94)
- Worthey, G., Trager, S. C., and Faber, S. M. 1996 in *Fresh Views of Elliptical Galaxies*, ed. A. Buzzoni, A. Renzini and A. Serrano (San Francisco: ASP) p. 203